Confidential manuscript submitted to *Advances in Space Research*

Title Page

Sea-Level Rise and Vertical Land Motion on the Islands of Oahu and Hawaii, Hawaii

Linqiang Yang[1] and Oceana Puananilei Francis[1, 2]

[1]Department of Civil and Environmental Engineering, University of Hawaii at Manoa, Honolulu, HI, USA.

[2]Sea Grant College Program, University of Hawaii at Manoa, Honolulu, HI, USA.

Corresponding author: Linqiang Yang

Email: Linqiang@hawaii.edu

Address: 2540 Dole Street, Holmes Hall 142A, Honolulu, HI 96822, USA

Co-author: Oceana Puananilei Francis

Email: oceanaf@hawaii.edu

Address: 2540 Dole Street, Holmes Hall 383, Honolulu, HI 96822, USA

Abstract

Sea-level rise is a highly publicized issue in the Hawaiian Islands because it is one of the main drivers for coastal hazards. In our study, multiple geodetic and in situ datasets are integrated to investigate the sea-level rise and vertical land motion on the islands of Oahu and Hawaii, Hawaii. The rates of relative sea-level changes are derived from the tide-gauge stations in the Hawaiian Islands, however the station located at Kawaihae, Hawaii presents a much higher trend than other stations. Our analysis shows that the questionable trend results from the sudden movement of the equipment on land, which is caused by a pair of earthquakes. After adjustment, we arrive at a revised and more consistent relative sea-level trend at this station. Our study shows that Oahu is vertically 'stable' (i.e., near-zero vertical land movement within uncertainties), and the relative sea-level change is dominated by the absolute sea-level change. However, the island of Hawaii was subsiding at -3.3±0.9 mm/year before 1973 and changed to -1.2±0.2 mm/year after 1975, which may relate to seismic activities and where relative sea-level change is attributed to both absolute sea-level change and vertical land motion. The difference in relative sea-level change between the islands of Oahu and Hawaii is due to the difference in vertical land motion rather than steric sea-level change. In addition, the ocean-mass components are the predominant factors that influence the long-term trends of absolute sea level on the islands of Oahu and Hawaii.

Keywords: Sea-level change; Tide gauge; Satellite altimetry; GRACE; GNSS; Time series analysis

1 Introduction

Sea-level rise poses a significant threat to the Hawaiian Islands because it exacerbates coastal hazards like inundation, coastal erosion, and flooding (Fletcher et al., 2010). A better understanding of sea-level rise is needed for the study of coastal hazards in the Hawaiian Islands. There are two techniques to measure the sea-level change: satellite altimetry and tide gauges. Satellite altimetry measures the sea-surface height relative to a reference ellipsoid, known as absolute sea level (ASL). Satellite altimetry can provide near-global measurements in the open ocean for studying sea-level changes, in comparison to tide gauges confined to the coasts (Francis et al., 2011). However, satellite altimetry provides high-precision data only within the last 25 years, which is too short to derive long-term trends as sea-level variations contain strong inter-decadal signals (Church and White, 2011; Douglas, 2001; Firing et al., 2004). Thus, estimates of long-term trends of sea level are largely dependent on a sparsely-distributed network of coastal and island tide gauges (Woodworth and Player, 2003). Tide gauges are usually placed on piers and measure the sea level relative to a nearby geodetic benchmark, known as relative sea level (RSL). RSL variation is comprised of two components: ASL variation and vertical land motion (VLM). Eq. (1) indicates the relationship of these three parts:

$$ASLT = RSLT + VLMR \tag{1}$$

where *ASLT* represents absolute sea-level trend, *RSLT* represents relative sea-level trend, and *VLMR* represents vertical land-motion rate. Therefore, it is impossible to distinguish whether the water is rising or the land is subsiding from the tide-gauge measurements alone (Yang et al., 2016b). Accounting for VLM is necessary when estimating the long-term trends of ASL from tide-gauge data. Currently, the Global Navigation Satellite System (GNSS) has proven to be a robust tool for VLM monitoring (Bouin and Wöppelmann, 2010; Wang and Soler, 2015;

Wöppelmann and Marcos, 2016; Yang et al., 2016a; Yang et al., 2016b). In our study, GNSS measurements obtained close to the tide gauges are employed to represent the VLM of the corresponding tide-gauge stations and, in turn, the long-term trends of ASL can be derived by combining tide-gauge and GNSS data.

Anderson et al. (2015) and Romine et al. (2013) investigated sea-level rise and its consequential impacts on coastal erosion in the Hawaiian Islands, by removing the average-seasonal-cycle signals when estimating the long-term trends of RSL from the tide-gauge data. Moore (1970, 1987) analyzed the tide-gauge data in Honolulu (HONO) and Hilo (HIHA) (Fig. 1(a) and Table 1) and indicated that Oahu was practically stable but the island of Hawaii was subsiding at a considerably faster rate, which dominated the difference of RSLT between the two islands. Caccamise et al. (2005) studied the difference of RSLT between Honolulu and Hilo by combining the data of tide gauges (HONO and HIHA) and nearby GNSS stations (HNLC-G and HILO-G respectively) (Fig. 1(a) and Table 1) and came up with a more complicated explanation. The 6-year GNSS measurements showed that the difference of VLMR (i.e., -0.4±0.4 mm/year) was too small to account for the difference of RSLT and the authors suggested that the rates of VLM had changed in Hilo but that variations in upper-ocean temperature could also explain much of the difference of RSLT. In our study, we analyze the differences of RSLT, VLMR, and steric sea-level (SSL) trends on and between the islands of Oahu and Hawaii with longer periods of data. We also include two more tide-gauge stations (MOKU and KAWA) (Fig. 1(a) and Table 1) for study of Oahu and Hawaii Islands, and an additional two stations (NAWI and KAHA) from Kauai and Maui Islands for estimation of regionally coherent noises (see Section 2.1). To enhance our analysis, we employ two additional types of datasets: satellite altimetry, and the Gravity Recovery and Climate Experiment (GRACE).

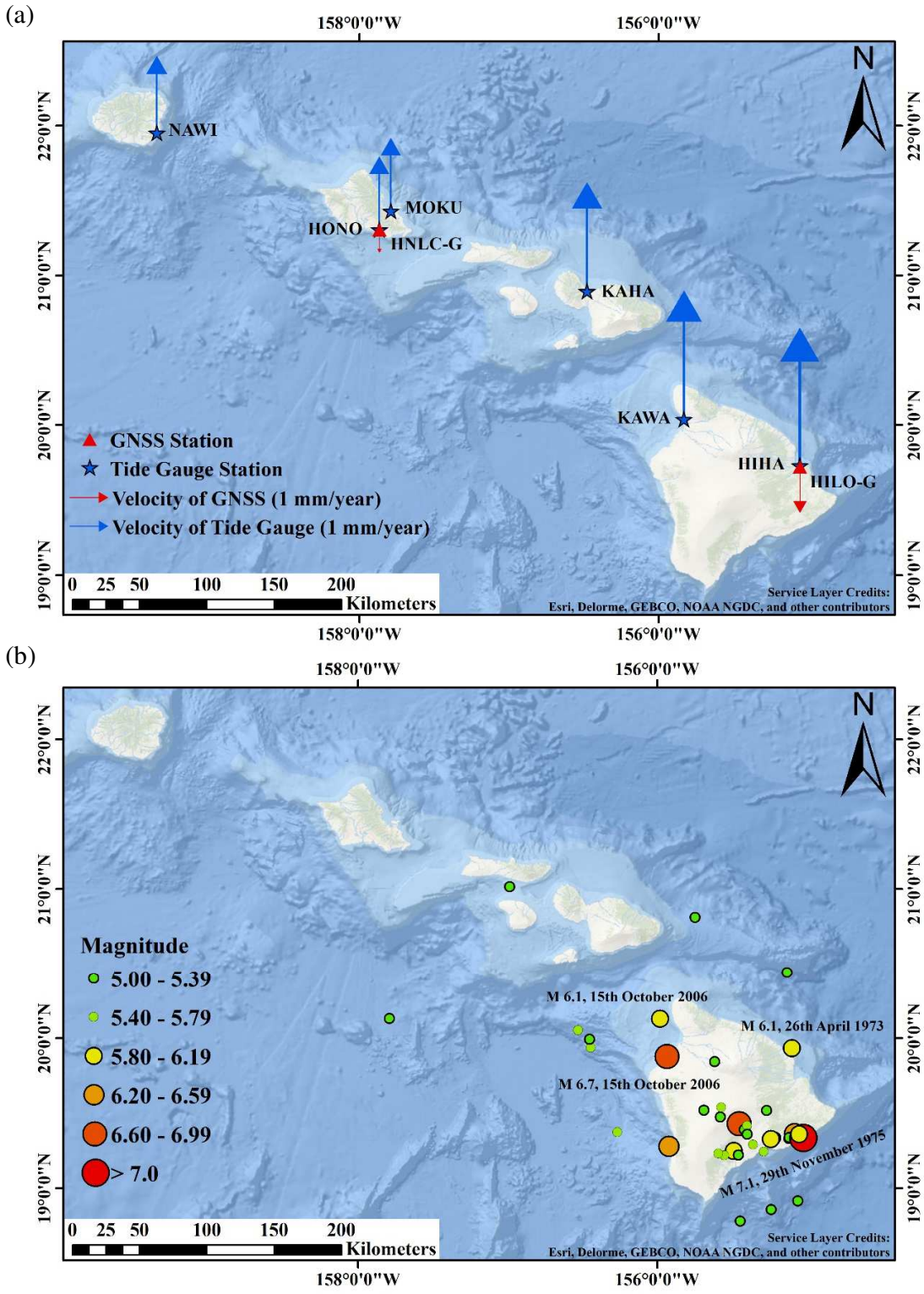

Figure 1. (a) Map showing the distribution of available tide-gauge and nearby GNSS stations in the Hawaiian Islands. Red triangles represent the locations of GNSS stations; blue stars represent the locations of tide-gauge stations; red arrows represent the vertical velocities of GNSS stations; and blue arrows represent the relative sea-level trends (RSLT) of tide-gauge stations. (b) Map

showing the distribution of earthquakes with magnitudes larger than 5.0 since 1951 in the Hawaiian Islands. Circles represent the locations and magnitudes of the earthquakes.

Table 1. Basic information of available tide-gauge and corresponding nearby GNSS stations in the Hawaiian Islands. Tide-gauge stations are given 4-character identifiers, while GNSS stations are indicated by a '-G' after their 4-character identifiers.

Tide Gauge						GNSS		Distance between Tide Gauge and GNSS (meter)
Station	Location	Latitude (ºNorth)	Longitude (ºEast)	Time Span	Completeness (%)	Station	Time Span	
NAWI	Nawiliwili Bay, Kauai Island	21.95	200.65	1955-2016	98.70	-	-	-
MOKU	Mokuoloe Island, Oahu Island	21.43	202.21	1957-2016	85.60	-	-	-
HONO	Honolulu, Oahu Island	21.31	202.13	1905-2016	100.00	HNLC-G	1997-2018	1
KAHA	Kahului Harbor, Maui Island	20.90	203.52	1947-2016	92.90	-	-	-
KAWA	Kawaihae, Hawaii Island	20.04	204.17	1988-2016	87.60	-	-	-
HIHA	Hilo, Hawaii Island	19.73	204.95	1927-2016	83.40	HILO-G	1997-2018	1300

2 Data and methods

2.1 Tide-Gauge Data

In this paper, we use monthly mean values of sea level provided by the Permanent Service for Mean Sea Level (PSMSL) (Holgate et al., 2013; PSMSL, 2018) to represent RSL. Fig. 1(a) and Table 1 present the distribution and basic information of the six available tide-gauge stations. Before estimating the long-term trends, the following process is applied. First, we employ monthly mean sea-level pressure (SLP) measurements from the National Centers for Environmental Prediction/National Center for Atmospheric Research (NCEP/NCAR) reanalysis data (Kalnay et al., 1996) for barometric pressure correction. The NCEP/NCAR SLP data span from January 1948 to December 2017 and the barometric pressure correction is applied to the overlapping period between the RSL and SLP time series. In order to keep the consistency of the data after correction, we only select the RSL time series that overlap with the SLP time series for further corrections and trend calculation. Second, we apply the Seasonal Trend Decomposition using Loess (STL) procedure to extract and remove the seasonal signals from the SLP-corrected RSL time series. The STL procedure was developed by Cleveland et al. (1990) and is a filtering procedure that employs a locally weighted regression (Yang et al., 2016a; Yang et al., 2016b). Third, we remove the common-mode-oceanographic signals from each RSL time series. The common-mode-oceanographic signals can be derived by averaging the monthly detrended and de-seasonalized RSL time series of all six available tide-gauge stations in the Hawaiian Islands (Fig. 1(a) and Table 1). Fourth, we use the ICE-6G_C(VM5a) model to make a Glacial Isostatic Adjustment (GIA) correction (Argus et al., 2014; Peltier et al., 2015). Finally, the linear trends are estimated using a software package called Hector (Bos et al., 2013) which can be used to estimate the trend in a time series with a temporally-correlated noise. It is well known that

temporal correlation exists in a time series of sea level, and neglecting it will significantly underestimate the uncertainty in estimated rates (Bos et al., 2014). There are various stochastic models available in Hector. In this study, we have compared four stochastic models, First-order Autoregressive (AR(1)), Fifth-order Autoregressive (AR(5)), Autoregressive Fractionally Integrated Moving Average (ARFIMA), and Generalized Gauss Markov (GGM), among which we have selected the one with the smallest ratio of Akaike Information Criterion (AIC) value to Bayesian Information Criterion (BIC) value (Bos and Fernandes, 2019). The uncertainties in the trends of the RSL time series are one standard error, 68% confidence interval.

2.2 GNSS Data

We make use of the daily GNSS data referenced to the global reference frame released by the International GNSS Service (IGS), called IGS08, to study the VLM of the islands of Oahu and Hawaii. The VLMR derived from GNSS data is reference frame-dependent. Therefore, an accurate and stable reference frame is needed for the study of the geocentric sea-level rise from GNSS-corrected tide gauge data due to the presence of the reference frame uncertainty (Collilieux and Wöppelmann, 2011). The latest release of the IGS reference frame is IGS14, which is based on the latest realization of the International Terrestrial Reference System (ITRS), namely ITRF2014 (Rebischung and Schmid, 2016; Altamimi et al., 2016). In this study, the GNSS data are downloaded from the Nevada Geodetic Laboratory (NGL), which uses the GIPSY/OASIS-II Version 6.1.1 software developed at the Jet Propulsion Laboratory (JPL) to process GNSS data from various archives (Blewitt et al., 2018). NGL has updated the reference frame of the GNSS data from IGS08 to IGS14 since 27th May 2018, while only the data processed after that date has been referenced to IGS14. Considering the consistency of the data, we only use the GNSS data referenced to the IGS08 in this study despite that IGS14 has higher

accuracy (Altamimi et al., 2016). Fig. 1(a) and Table 1 show the locations and information of the two GNSS stations (HNLC-G and HILO-G) which are located near to the Honolulu and Hilo tide gauges, respectively. Caccamise et al. (2005) indicated that the vertical velocities observed at HNLC-G and HILO-G could represent the VLM of the corresponding nearby tide-gauge stations respectively. In our study, what we call HILO-G represents the combined GNSS time series of two individual GNSS records: HILO-G itself and also HILR-G. Because the termination date of the HILO-G record (27th April 2010) is almost the start date of the HILR-G record (25th May 2010), and the two stations are only 500 meters apart, we combine HILO-G and HILR-G records to get a longer time series under the assumption that they are located on the same bedrock. For the purpose of obtaining a precise estimate of the trend of GNSS time series, the following steps are applied. First, we detect and remove the outliers in the GNSS time series. Second, we adjust the offsets in the GNSS time series. Offsets are known to exist in GNSS time series, and they may have a detrimental effect on VLMR estimation depending on their sizes and locations in the GNSS time series (Gazeaux et al., 2013). In order to obtain reliable velocity estimates, the offsets occurring at known times (e.g., documented equipment changes and earthquakes recorded by NGL) in the time series are adjusted by applying the software Hector which fits the Heaviside step function to data (Bos et al., 2013). In this study, because HILO-G represents the combined data of HILO-G and HILR-G, the start time of HILR-G is also set as an offset point and an adjustment of 1513.4 mm is applied. To confirm the assumption that the two GNSS stations, HILO-G and HILR-G, are located on the same bedrock and validate the estimate of the offset (i.e., 1513.4 mm), we recommend carrying out a series of levelling campaigns between the two stations, and in turn, the GNSS records can be rigorously combined for future studies. Third, we employ the Singular Spectrum Analysis (SSA) method to extract the seasonal signals and in turn

remove it from the GNSS time series. SSA is a data-driven technique that can extract useful information from noisy time series without prior knowledge of the dynamics affecting the time series (Chen et al., 2013; Hassani, 2007; Wang et al., 2016). Finally, the GNSS time series trend can be derived by using Hector (Bos et al., 2013). The GNSS time series also has a temporally-correlated noise. For example, previous studies such as those of Zhang et al. (1997), Mao et al. (1999), and Hackl et al. (2011) suggest that the noise is a combination of flicker, random walk , and white noise. Therefore, these three stochastic models are considered when estimating the trends of the GNSS time series and the uncertainties in the trends are one standard error, 68% confidence interval.

2.3 Satellite Altimetry Data

We use the reprocessed and merged-gridded sea-level-anomaly heights for global areas processed by Ssalto/Duacs (Mertz et al., 2018) to represent the ASL in our study. The sea-level-anomaly data were corrected for dry and wet troposphere, ocean tide, pole tide, solid earth tide, loading tide, sea state bias, orbit error, and Dynamic Atmospheric Correction (DAC) (Pujol and Sea Level Thematic Center Team, 2017). The dataset has a spatial grid resolution of 0.25×0.25 degrees and is projected onto a Cartesian grid with respect to a 20-year reference period (1993-2012). The data, which are given by monthly-averaged values, span the period 1st January 1993 to 15th May 2017. Before estimating the trends of ASL with Hector, the data are processed in the following way. First, the seasonal signals are extracted using STL procedure and, in turn, removed from the time series for each grid point. Second, the common-mode-oceanographic signals are constructed and removed from the time series for each grid point. Here, the method implemented to derive the common-mode-oceanographic signals is slightly different with that introduced in Section 2.1. For each target grid point, the common-mode-oceanographic signals

are constructed by averaging the detrended and de-seasonalized time series of selected grid points. The selected grid points should be within a 5-degree radius from the target grid point and the correlation coefficients between the target and selected grid points should be greater than the average correlation coefficient of all pairs of grid points in the Hawaii area. Third, the ASL time series associated with the tide-gauge stations are determined by interpolating the gridded data and the ICE-6G_C(VM5a) model is employed to remove the GIA effect (Argus et al., 2014; Peltier et al., 2015). Finally, a stochastic model is determined according to the method presented in Section 2.1 and the trend can be estimated using Hector. The uncertainties in the trends of the ASL time series are one standard error, 68% confidence interval.

2.4 GRACE Data

We employ the CSR GRACE RL05 Mascon solutions from the Center for Space Research (CSR) at the University of Texas, Austin, to represent the sea-level change caused by the ocean-mass change (Save et al., 2016). In the GRACE data, the sea-level change due to the ocean-mass change is represented by a variable called equivalent water thickness. The estimated global mascon solutions have the C_{20} (degree 2 order 0) coefficients which explains the oblateness, and it is substituted with the C_{20} solutions from Satellite Laser Ranging (SLR) (Cheng et al., 2013) to be consistent with the other GRACE solutions; the degree 1 coefficients (C_{11}, S_{11} and C_{10}) are corrected using the method presented by Swenson et al. (2008); the Mascon solutions have also applied the GIA correction based on the model from A et al. (2013); the GRACE anomalies reported in the Mascon solutions are relative to a mean baseline between 2004.000 to 2009.999 (Save et al., 2016). The Mascon solutions are represented on a 0.5×0.5 degrees longitude-latitude grid, but they represent an area equal to that of a geodesic grid of size 1×1 degree at the equator. The monthly datasets span the period 17th April 2002 to 10th June 2017. The ocean mass time

series, associated with tide-gauge stations, are derived by interpolating the gridded data. The trends are estimated using Hector, after removing seasonal signals which are extracted using STL procedures and adding a stochastic model which is determined by the method mentioned in Section 2.1 into the estimation process. The uncertainties in the trends of the ocean mass time series are one standard error, 68% confidence interval.

2.5 Temperature and Salinity Data

The EN4.2.1 objective analyses data produced and maintained by the Met Office Hadley Centre are used to estimate the trends of SSL in our study. The data are a collection of ocean temperature and salinity profiles across the global oceans, from 1900 to present, with a series of quality control checks applied (Good et al., 2013). The data are distributed in a grid with a spatial resolution of 1×1 degree, and every point has 42 levels in the vertical (from 5 meters to 5350 meters). Due to the data availability and distribution, we only use the monthly datasets from 1st January 1947 to 1st December 2017 and the first 38 levels (from 5 meters to 4155 meters) in depth. The Gibbs-SeaWater (GSW) Oceanographic Toolbox (McDougall and Barker, 2011) is applied to calculate the SSL and the gridded data are interpolated to the tide-gauge locations. Finally, the long-term trends are estimated using Hector after eliminating seasonal signals derived by using STL procedures and adding a stochastic model which can be determined by the method mentioned in Section 2.1 into the estimation process. The uncertainties in the trends of the SSL time series are one standard error, 68% confidence interval.

3 Results and discussion

3.1 Sea-Level Rise and Vertical Land Motion on Oahu

The RSLT at MOKU and HONO stations and the RSLT difference (MOKU-HONO) in their common periods (1957–2016) are shown in Fig. 2(a), Table 2, and Table 3. MOKU station shows a rate of 1.8±0.3 mm/year during 1957–2016, and HONO station shows a rate of 1.8±0.3 mm/year during 1948–2016. The RSLT at the two stations are both close to the global mean sea-level rise rate, 1.7±0.2 mm/year during 1900–2009 presented by Church and White (2011), which supports the notion that Oahu is vertically 'stable' (i.e., near-zero vertical land movement within uncertainties). Fig. 4(b) and Table 2 present the rate of VLM at HONO station measured by the nearby GNSS station HNLC-G (see Section 3.3). It shows that HNLC-G is subsiding at a rate of 0.4±0.3 mm/year during 1997–2018, which is similar to the subsidence rates presented by Blewitt et al. (2016) (0.7±0.8 mm/year) and Santamaría-Gómez et al. (2017) (0.2±0.3 mm/year). The VLMR at HNLC-G station (-0.4±0.3 mm/year) shows no statistically significant subsidence and should be regarded as 'stable' (i.e., near-zero vertical land movement within uncertainties) rather than moving. For the MOKU station, there is no nearby GNSS station to provide the VLM information directly, but it can be estimated by combining ASLT and RSLT according to Eq. (1). The drawback of this method is that the estimated VLMR is limited by the ASLT derived from the short satellite altimetry data with short-term (inter-annual, decadal and interdecadal) variability (Santamaría-Gómez et al., 2014). To reduce the uncertainty and remove the common-trend errors and most of the spatially-correlated signals, the following approach is applied:

$$\begin{aligned} \Delta VLMR &= VLMR_2 - VLMR_1 \\ &= ASLT_2 - RSLT_2 - ASLT_1 + RSLT_1 = \Delta ASLT - \Delta RSLT \end{aligned} \tag{2}$$

where $\Delta VLMR$ is the difference of VLMR between two tide-gauge stations, $\Delta ASLT$ is the difference of ASLT between two tide-gauge stations, and $\Delta RSLT$ is the difference of RSLT

between two tide-gauge stations. The VLMR at MOKU station is derived by combining the VLMR at HONO and the $\Delta VLMR$ calculated from Eq. (2). Fig. 2(a) and Table 3 show that the $\Delta RSLT$ between MOKU and HONO stations is 0.1±0.1 mm/year. Fig. 2(b) shows that the ASLT at MOKU and HONO stations are the same, 2.1±1.2 mm/year, and the $\Delta ASLT$ (MOKU-HONO) is -0.0±0.03 mm/year. Therefore, the $\Delta VLMR$ is -0.1±0.1 mm/year, and the VLMR at MOKU station is -0.5±0.3 mm/year, which is considered 'stable' (i.e., near-zero vertical land movement within uncertainties) in our study. The VLMR results at both Honolulu and Mokuoloe Island provide support towards Oahu being vertically 'stable' (i.e., near-zero vertical land movement within uncertainties). Thus, the data point towards the conclusion that the RSL change on Oahu is dominated by the ASL change, rather than the VLM.

Table 2. Rates of sea-level change estimated from tide gauge, satellite altimetry, GRACE, and temperature and salinity data at tide-gauge stations and rates of vertical land motion estimated from nearby GNSS stations. The given rates are in mm/year and uncertainties are one standard error.

Tide Gauge ID	Relative Sea-Level Trend	Absolute Sea-Level Trend (1993-2017)	Ocean Mass Change Rate (2002-2017)	Steric Sea-Level Trend (1947-2017)	Vertical Land-Motion Rate (1997-2018)
MOKU	1.8±0.3[a]	2.1±1.2	3.5±0.2	0.1±0.3	
HONO	1.8±0.3[a]	2.1±1.2	3.5±0.2	0.1±0.3	-0.4±0.3
KAWA	3.2±1.0[a]	1.3±1.3	3.4±0.2	-0.1±0.3	
HIHA	3.5±0.3[a] 4.7±1.1[b] 3.0±0.7[c]	2.1±1.6	3.3±0.1	-0.1±0.3	-1.2±0.2

[a]Relative sea-level trends are estimated from corrected tide-gauge data that overlap with the sea level pressure time series at each tide-gauge station, i.e., MOKU: 1957-2016, HONO: 1948-2016, KAWA: 1988-2016, and HIHA: 1948-2016 (see Section 2.1).
[b]Relative sea-level trend is estimated over the period 1948-1973 at HIHA station.
[c]Relative sea-level trend is estimated over the period 1975-2016 at HIHA station.

Table 3. Differences of sea-level trends obtained by differencing data from tide gauge, satellite altimetry, GRACE, and temperature and salinity at tide-gauge stations, respectively, and difference of vertical land-motion rates obtained by differencing data from nearby GNSS stations[a]. The given rates are in mm/year and uncertainties are one standard error.

Compared Tide Gauge Stations	Relative Sea-Level Trend Difference	Absolute Sea-Level Trend Difference (1993-2017)	Ocean Mass Change Rate Difference (2002-2017)	Steric Sea-Level Trend Difference (1947-2017)	Vertical Land-Motion Rate Difference (1997-2018)
MOKU-HONO	0.1±0.1[b]	-0.0±0.03	-0.0±0.01	0.0±0.02	
KAWA-HIHA	0.3±0.4[b]	-0.4±0.3	0.1±0.02	-0.1±0.04	
HIHA-HONO	1.5±0.2[b]	-0.2±0.6	-0.2±0.1	-0.1±0.1	-0.7±0.2
	2.7±0.6[c]			1.0±0.5[e]	
	0.9±0.3[d]			-0.3±0.3[f]	

[a]Differences of sea-level trends are estimated from the differenced data over the common periods of compared tide-gauge stations and difference of vertical land-motion rates is estimated from the differenced data over the common periods of nearby GNSS stations.
[b]Relative sea-level trend differences are estimated over the common periods of compared tide-gauge stations, i.e., MOKU-HONO: 1957-2016, KAWA-HIHA: 1988-2016, and HIHA-HONO: 1948-2016.
[c]Relative sea-level trend difference is estimated over the period 1948-1973 between HIHA and HONO stations.
[d]Relative sea-level trend difference is estimated over the period 1975-2016 between HIHA and HONO stations.
[e]Steric sea-level trend difference is estimated over the period 1947-1973 between HIHA and HONO stations.
[f]Steric sea-level trend difference is estimated over the period 1975-2017 between HIHA and HONO stations.

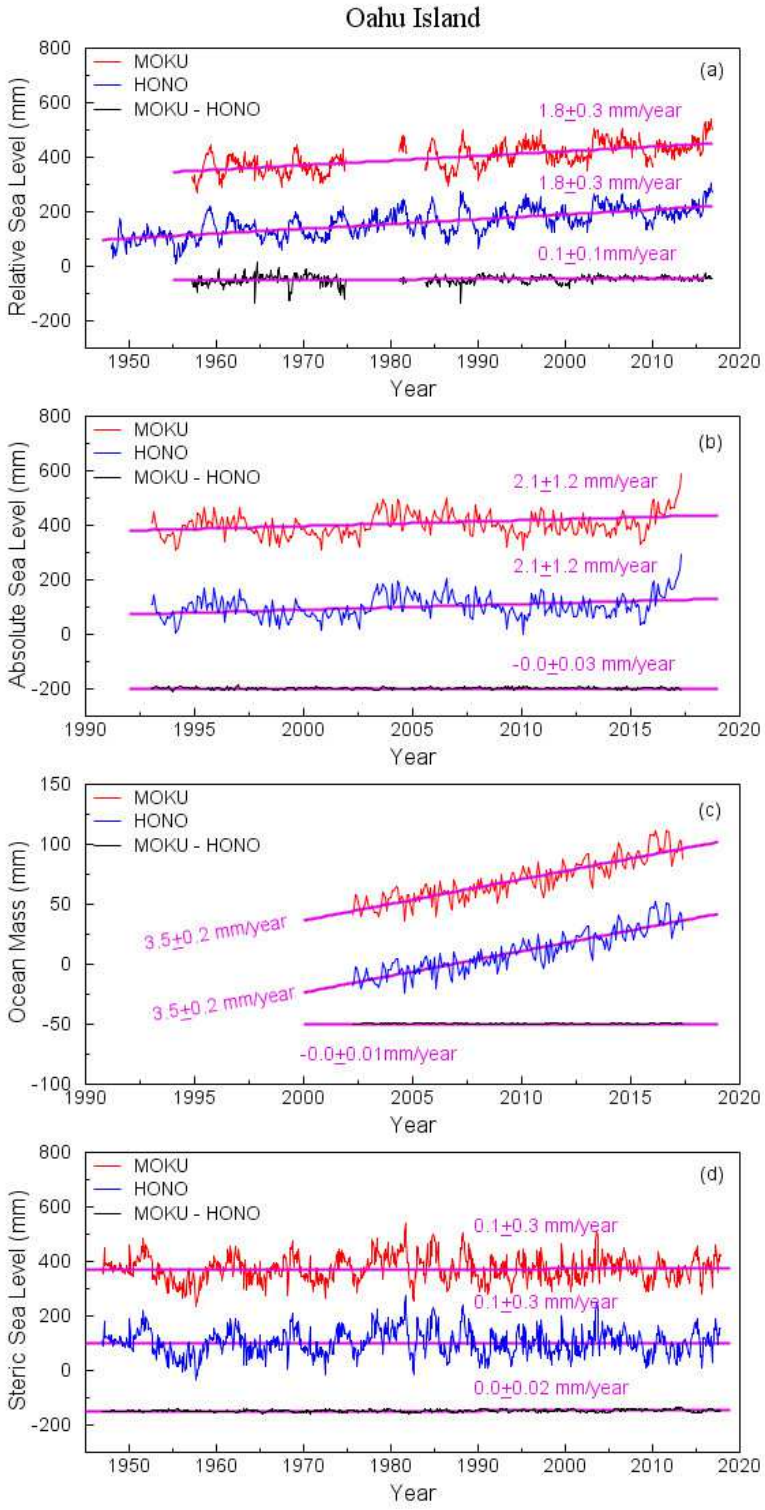

Figure 2. Plots showing the sea-level trends and trend differences at and between MOKU and HONO stations utilizing different datasets for (a) relative sea level (RSL) from tide gauges; (b) absolute sea level (ASL) from satellite altimetry; (c) ocean mass from GRACE; and (d) steric sea level (SSL) from temperature and salinity data. The magenta lines represent linear trends. The

mean values have been removed from all the time series, respectively, and the time series are displayed with arbitrary offsets for presentation purposes.

In our study, we further investigate the ASL change and its two major components: SSL change dominated by the heat and salinity contents and ocean-mass change from the water exchange between the oceans and other reservoirs at MOKU and HONO stations (Leuliette and Miller, 2009). MOKU and HONO stations have the same rate of ocean-mass change during 2002–2017, 3.5±0.2 mm/year, and a trend difference (MOKU-HONO) of -0.0±0.01 mm/year, as shown in Fig. 2(c). Fig. 2(d) presents the SSL trend at MOKU and HONO stations and the trend difference (MOKU-HONO) during 1947–2017, where both stations have rates that are close to zero, i.e., 0.1±0.3 mm/year at MOKU and 0.1±0.3 mm/year at HONO, and a trend difference of 0.0±0.02 mm/year. The results indicate that the rates of ASL change, SSL change, and ocean-mass change are all similar between MOKU and HONO stations. It should be noted that the distance between MOKU and HONO stations is smaller than the grid sizes of the GRACE and temperature and salinity data. Therefore, it would be expected that the two stations have similar SSL and ocean-mass changes. The ASLT difference (-0.0±0.03 mm/year) derived from satellite altimetry matches well with that derived from the combination of ocean-mass and steric components (0.0±0.02 mm/year) within a 68% confidence interval. Although the duration of the three types of data is different, especially with the GRACE data having only a length of 16 years, which is too short to estimate the long-term trend, it still suggests that the long-term trends of ASL at MOKU and HONO are dominated by the ocean-mass components since the long-term trends of the SSL at both stations are close to zero, as shown in Fig. 2(d) and Table 2.

3.2 Sea-Level Rise and Vertical Land Motion on the Island of Hawaii

Fig. 3(a) presents the original RSLT at KAWA and HIHA stations. KAWA station has a more rapidly rising rate, 7.2±1.2 mm/year during 1988–2016, compared to HIHA station, 3.5±0.3 mm/year, during 1948–2016. But the RSLT difference (KAWA-HIHA), during 1988–2016, presents an obvious discontinuity (jump) in October 2006, as shown in Fig. 3(b). The RSLT differences are almost the same within uncertainties before and after the jump, 0.3±0.9 mm/year versus 0.8±0.6 mm/year, respectively. The sharp change can be attributed to sudden movement of equipment on land, because it is nearly impossible for ASL change to generate such an offset (i.e., 86.4 mm) in one month in the differenced RSL time series between two tide gauge stations located on the same island. Fig. 1(b) shows that most seismic activities, which are closely related to volcanism, occurred on the island of Hawaii (Fletcher et al., 2010), among which a pair of earthquakes with magnitudes of 6.7 and 6.1 occurred on the same day (15th October 2006) near Kawaihae, Hawaii. We surmise that the sudden jump in the RSL difference results from the abrupt movement of equipment on land at KAWA station, which is caused by the earthquakes. Because the offset has a detrimental effect on the trend estimation of RSL at KAWA station, we use Hector which fits the Heaviside step function to data to estimate the offset and an adjustment of 86.4 mm is applied to the RSL data at KAWA station after October 2006. After the correction, the correlation of RSL between KAWA and HIHA stations increases from 0.79 to 0.95. KAWA station shows an RSLT of 3.2±1.0 mm/year during 1988–2016 (Fig. 3(a) and Table 2), and an RSLT difference (KAWA-HIHA) of 0.3±0.4 mm/year (Fig. 3(b) and Table 3).

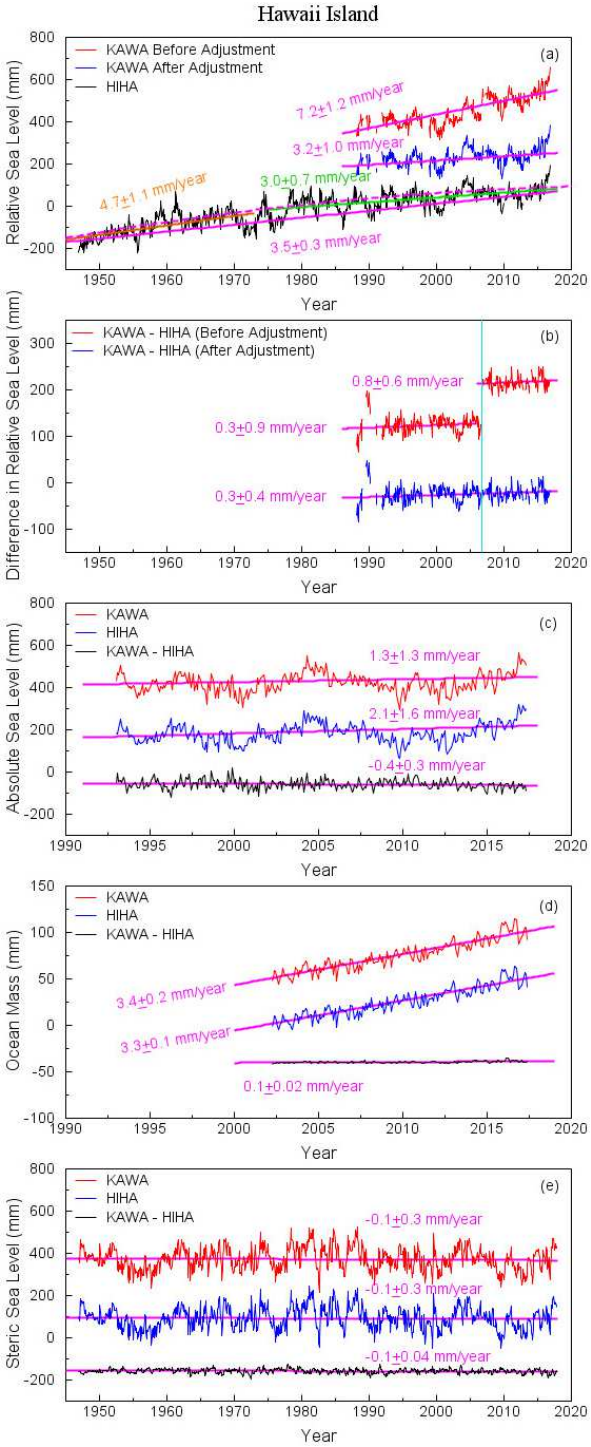

Figure 3. Plots showing the sea-level trends and trend differences at and between KAWA and HIHA stations utilizing different datasets for (a) relative sea level (RSL) from tide gauges, the orange line represents the trend during 1948–1973, the green line represents the trend during 1975–2016, the magenta dashed line represents quadratic dependence; (b) difference in relative sea level (RSL) before and after adjustment, the cyan line represents the date of October 2006; (c) absolute sea level (ASL) from satellite altimetry; (d) ocean mass from GRACE; and (e) steric

sea level (SSL) from temperature and salinity data. The magenta lines represent linear trends. The mean values have been removed from all the time series, respectively, and the time series are displayed with arbitrary offsets for presentation purposes.

Caccamise et al. (2005) indicated that the RSLT of HIHA station changed around 1975, which might result from the subsidence-rate change of Hilo. In Fig. 3(a), the quadratic dependence of HIHA station supports the notion that the RSLT has changed around 1975. Figure 3(a) and Table 2 present the RSLT change at the HIHA station from 4.7±1.1 mm/year during 1948–1973 to 3.0±0.7 mm/year during 1975–2016. We surmise that the trend change of RSL at the HIHA station is attributed to the rate change of VLM, which is possibly associated with the two large damaging earthquakes occurring near Hilo around 1975 as shown in Fig. 1(b): one occurred 15 km north of Hilo, Hawaii at a focal depth of 48 km on 26th April 1973, with a magnitude of 6.1 (Butler, 1982), and the other took place on the south flank of Kilauea Volcano, which triggered the largest locally-generated Hawaii tsunami in modern times on 29th November 1975, with a magnitude of 7.1 (Fletcher et al., 2010). The results, shown in Fig. 3(a) and Table 2, suggest that the island of Hawaii is experiencing subsidence since the RSLT of HIHA station (1948–1973: 4.7±1.1 mm/year, 1975–2016: 3.0±0.7 mm/year, 1948–2016: 3.5±0.3 mm/year) and KAWA station (1988–2016: 3.2±1.0 mm/year) are all greater than the global mean sea-level rate (1.7±0.2 mm/year during 1900–2009 presented by Church and White (2011)). Fig. 4(b) and Table 2 indicate that HIHA station is subsiding at a rate of 1.2±0.2 mm/year, as measured by the nearby GNSS station HILO-G during 1997–2018 (see Section 3.3). The VLMR of HILO-G (-1.2±0.2 mm/year), obtained in this study, is similar to the results presented by Blewitt et al. (2016) (-1.4±1.0 mm/year) and Santamaría-Gómez et al. (2017) (-1.1±0.3 mm/year). According to the method introduced in Section 3.1, the VLMR of KAWA station is -1.9±0.5 mm/year. The VLM results of HIHA and KAWA stations provide evidence that this part of the island of

Hawaii is subsiding. Our results indicate that the RSL change at KAWA station is dominated by the VLM during 1988–2016, but the ASL change contributes more to the RSL change at HIHA station during 1975–2016.

Fig. 3(c) and Table 2 present the trends of ASL at KAWA and HIHA stations during 1993–2017. It shows that the two stations have similar rising rates (HIHA: 2.1±1.6 mm/year versus KAWA: 1.3±1.3 mm/year) within a 68% confidence interval. Figs 3(d) and (e) show the ocean-mass and steric components of ASL at KAWA and HIHA stations, respectively. Both components have near-zero trend differences (KAWA-HIHA), 0.1±0.02 mm/year in ocean-mass component and -0.1±0.04 mm/year in SSL component. It should be noted that the distance between KAWA and HIHA stations is close to the grid sizes of the GRACE and temperature and salinity data. Therefore, it would be expected that the two stations have similar SSL and ocean-mass changes. The trend difference of ASL (KAWA-HIHA: -0.4±0.3 mm/year), derived from satellite altimetry, compares well with that derived from the combination of ocean-mass and steric components (0.0±0.04 mm/year) within a 68% confidence interval. The ocean-mass components at both KAWA and HIHA stations are the predominant factors that affect the long-term ASLT compared to the steric components, which have near-zero trends.

3.3 Sea-Level Rise and Vertical Land Motion between the Islands of Oahu and Hawaii

The RSLT of HIHA and HONO stations and the trend difference (HIHA-HONO: 1.5±0.2 mm/year during 1948–2016) are shown in Fig. 4(a), Table 2, and Table 3. The RSL difference shows a trend change that decreases from 2.7±0.6 mm/year (1948–1973) to 0.9±0.3 mm/year (1975–2016), which results from the trend change in RSL at the HIHA station, as discussed in Section 3.2. Fig. 4(b) and Table 2 present the VLMR of HIHA and HONO stations derived from the nearby GNSS stations, HILO-G and HNLC-G, respectively. It shows that HILO-G (-1.2±0.2

mm/year) is subsiding at a faster rate compared to HNLC-G (-0.4±0.3 mm/year) during 1997–2018. The VLMR difference (HILO-G-HNLC-G) shows a rate of -0.7±0.2 mm/year within a 68% confidence interval during 1997–2018, which is larger than the result (i.e., -0.4±0.4 mm/year within a 95% confidence interval during 1996–2002) presented by Caccamise et al. (2005). The discrepancy may be a result from the difference in duration of the data used and software applied to process the data. The GNSS data used in our study are 16 years longer compared to those used by Caccamise et al. (2005). The GNSS data used in our study are processed by the GIPSY/OASIS-II Version 6.1.1 software which provides absolute positioning (Blewitt et al., 2018), while Caccamise et al. (2005) use GAMIT/GLOBK software, Release 10.0, which provides relative positioning. Our result shows that the VLMR difference (-0.7±0.2 mm/year, noting that a negative VLMR corresponds to a positive RSLT) during 1997–2018 can reconcile the RSLT difference (0.9 ±0.3 mm/year) well during 1975–2016, but is too small to account for the RSLT difference (2.7±0.6 mm/year) during 1948–1973. This may be attributed to the rate change of VLM at Hilo, relating to the seismic activities that occurred in 1973 and 1975. Fig. 4(c) and Table 2 present the ASLT of HIHA and HONO stations during 1993–2017. The two stations have similar ASLT (HIHA: 2.1±1.6 mm/year versus HONO: 2.1 ±1.2 mm/year), and a trend difference (HIHA-HONO) of -0.2±0.6 mm/year. Under the admittedly large assumption that the long-term ASL changes linearly, the VLMR of HIHA station before 1973 is derived according to the method presented in Section 3.1. The $\Delta VLMR$ between HIHA and HONO stations before 1973 is estimated as -2.9±0.8 mm/year using Eq. (2), and, in turn, the VLMR of HIHA station before 1973 is -3.3±0.9 mm/year. Caccamise et al. (2005) indicated that the difference in SSL trend might contribute greatly to the RSLT difference between the two stations. However, our result shows that the SSL trend difference (HIHA-HONO) is marginal

during 1947–2017, with a rate of -0.1±0.1 mm/year, compared to that of the RSLT difference (1.5±0.2 mm/year) during 1948–2016, as shown in Fig. 4(e) and Table 3. When dividing the time series into two parts, the trend differences of RSL are both dominated by the VLMR differences rather than the SSL trend differences, -2.9±0.8 mm/year versus 1.0±0.5 mm/year before 1973, and -0.7±0.2 mm/year versus -0.3±0.3 mm/year after 1975.

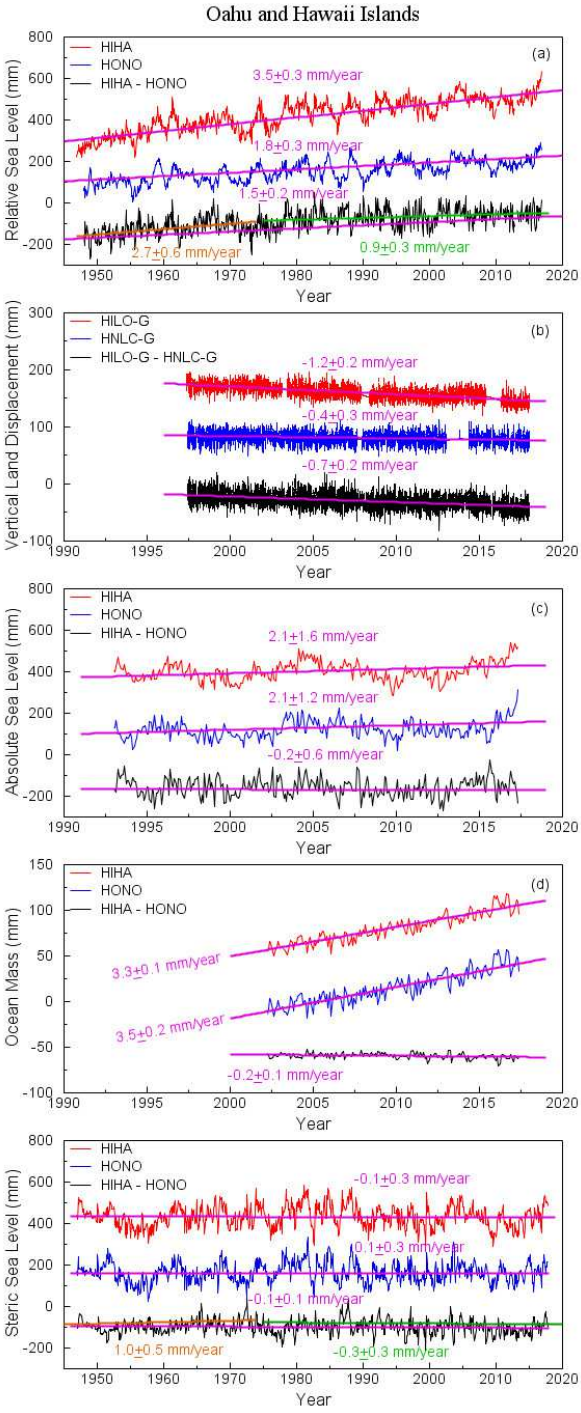

Figure 4. Plots showing the trends and trend differences of sea level and vertical land-motion rate (VLMR) and rate difference at and between HIHA and HONO stations utilizing different datasets for (a) relative sea level (RSL) from tide gauges, the orange line represents the trend during 1948–1973, the green line represents the trend during 1975–2016 ; (b) vertical land motion (VLM) from GNSS; (c) absolute sea level (ASL) from satellite altimetry; (d) ocean mass from GRACE; and (e) steric sea level (SSL) from temperature and salinity data, the orange line represents the trend during 1947–1973, the green line represents the trend during 1975–2017.

The magenta lines represent the linear trends. The mean values have been removed from all the time series, respectively, and the time series are displayed with arbitrary offsets for presentation purposes.

Fig. 4(c) and Table 2 show that HIHA and HONO stations have similar ASLT during 1993–2017. Figs 4(d) and (e) present the ocean-mass and steric components of ASL. For the ocean-mass component, the rise at the HIHA station is slower compared to HONO station during 2002–2017 with a trend difference of -0.2±0.1 mm/year. For steric component, the two stations have similar rates, with a trend difference of -0.1±0.1 mm/year during 1947–2017. The trend difference for ASL (-0.2±0.6 mm/year), derived from satellite altimetry, matches well with that derived from the combination of ocean-mass and steric components (-0.3±0.1 mm/year), within a 68% confidence interval.

4 Conclusion

Our study analyzes the sea-level rise and VLM on the islands of Oahu and Hawaii, Hawaii using integrated geodetic and in situ data. We identify and correct the questionable RSLT at KAWA station located on the island of Hawaii, which is probably due to a pair of earthquakes that occurred in 2006. The trend decreases from 7.2±1.2 mm/year to 3.2±1.0 mm/year over the period 1988–2016, after the correction. The RSL change and VLM results demonstrate that Oahu is vertically 'stable' (i.e., near-zero vertical land movement within uncertainties), but the island of Hawaii is subsiding with varied rates, -3.3±0.9 mm/year before 1973 and -1.2±0.2 mm/year after 1975, which probably results from two seismic activities that occurred in 1973 and 1975. The RSL change on Oahu is dominated by the ASL change but attributes to both ASL change and VLM for the island of Hawaii. The VLMR difference, rather than the SSL trend difference, accounts for much of the RSLT difference between the islands of Oahu and Hawaii. Furthermore, the long-term trends of ASL on the islands of Oahu and Hawaii are dominated by

the ocean-mass change. It is expected that our study will improve the understanding of sea-level rise and sea-level rise related hazards for the Hawaiian Islands.

Acknowledgments

Our study was supported by the State of Hawaii Department of Transportation, HWY-06-16, entitled 'Statewide Highway Shoreline Protection Program Study Update'. We acknowledge the Coastal Hydraulics Engineering Resilience (CHER) Laboratory at the University of Hawaii at Manoa. The tide-gauge data can be downloaded from the Permanent Service for Mean Sea Level (PSMSL) (https://www.psmsl.org/). The sea-level pressure data are provided by the NOAA/OAR/ESRL PSD, Boulder, Colorado, USA (http://www.esrl.noaa.gov/psd/). The GNSS data are available at the Nevada Geodetic Laboratory (NGL) (http://geodesy.unr.edu/NGLStationPages/GlobalStationList). The satellite altimetry data are accessible at the Copernicus Marine Environment Monitoring Service (CMEMS) (http://marine.copernicus.eu/). The GRACE data are released by the Center for Space Research (CSR) at the University of Texas, Austin (http://www2.csr.utexas.edu/grace/RL05_mascons.html). The temperature and salinity data are available at the Met Office Hadley Centre (https://www.metoffice.gov.uk/hadobs/en4/download-en4-2-1.html). We thank Philip Thompson and Chip Fletcher, at the University of Hawaii at Manoa, for their thoughtful conversations regarding our study.

References

A, G., Wahr, J., and Zhong, S. (2013). Computations of the viscoelastic response of a 3-D compressible Earth to surface loading: an application to Glacial Isostatic Adjustment in Antarctica and Canada. *Geophysical Journal International*, *192*(2), 557-572. https://doi.org/10.1093/gji/ggs030

Altamimi, Z., Rebischung, P., Métivier, L., and Collilieux, X. (2016). ITRF2014: A new release of the International Terrestrial Reference Frame modeling nonlinear station motions. *Journal of Geophysical Research: Solid Earth*, *121*(8), 6109–6131. https://doi.org/10.1002/2016JB013098

Anderson, T. R., Fletcher, C. H., Barbee, M. M., Frazer, L. N., and Romine, B. M. (2015). Doubling of coastal erosion under rising sea level by mid-century in Hawaii. *Natural Hazards*, *78*(1), 75–103. https://doi.org/10.1007/s11069-015-1698-6

Argus, D. F., Peltier, W. R., Drummond, R., and Moore, A. W. (2014). The Antarctica component of postglacial rebound model ICE-6G_C (VM5a) based on GPS positioning, exposure age dating of ice thicknesses, and relative sea level histories. *Geophysical Journal International*, *198(1)*, 537–563. https://doi.org/10.1093/gji/ggu140

Blewitt, G., Hammond, W. C., and Kreemer, C. (2018). Harnessing the GPS data explosion for interdisciplinary science. *Earth and Space Science News*, *99*. https://doi.org/10.1029/2018EO104623

Blewitt, G., Kreemer, C., Hammond, W. C., and Gazeaux, J. (2016). MIDAS robust trend estimator for accurate GPS station velocities without step detection. *Journal of Geophysical Research: Solid Earth*, *121*(3), 2054–2068. https://doi.org/10.1002/2015JB012552

Bos, M. S., and Fernandes, R. M. S. (2019). Hector user manual (Version 1.7.2). *Space and Earth Geodetic Analysis Laboratory*. Retrieved from http://segal.ubi.pt/hector/manual_1.7.2.pdf

Bos, M. S., Fernandes, R. M. S., Williams, S. D. P., and Bastos, L. (2013). Fast error analysis of continuous GNSS observations with missing data. *Journal of Geodesy*, *87*(4), 351–360. https://doi.org/10.1007/s00190-012-0605-0

Bos, M. S., Williams, S. D. P., Araújo, I. B., and Bastos, L. (2014). The effect of temporal correlated noise on the sea level rate and acceleration uncertainty. *Geophysical Journal International*, *196*(3), 1423–1430. https://doi.org/10.1093/gji/ggt481

Bouin, M. N., and Wöppelmann, G. (2010). Land motion estimates from GPS at tide gauges: A geophysical evaluation. *Geophysical Journal International*, *180*(1), 193–209. https://doi.org/10.1111/j.1365-246X.2009.04411.x

Butler, R. (1982). The 1973 Hawaii earthquake: a double earthquake beneath the volcano Mauna Kea. *Geophysical Journal International*, *69*(1), 173–186. https://doi.org/10.1111/j.1365-246X.1982.tb04942.x

Caccamise, D. J., Merrifield, M. A., Bevis, M., Foster, J., Firing, Y. L., Schenewerk, M. S., Taylor, F. W., and Thomas, D. A. (2005). Sea level rise at Honolulu and Hilo, Hawaii: GPS estimates of differential land motion. *Geophysical Research Letters*, 32, L03607. https://doi.org/10.1029/2004GL021380

Chen, Q., van Dam, T., Sneeuw, N., Collilieux, X., Weigelt, M., and Rebischung, P. (2013). Singular spectrum analysis for modeling seasonal signals from GPS time series. *Journal of Geodynamics*, *72*, 25–35. https://doi.org/10.1016/j.jog.2013.05.005

Cheng, M., Tapley, B. D., and Ries, J. C. (2013). Deceleration in the Earth's oblateness. *Journal of Geophysical Research: Solid Earth*, *118*(2), 740–747. https://doi.org/10.1002/jgrb.50058

Church, J. A., and White, N. J. (2011). Sea-Level Rise from the Late 19th to the Early 21st Century. *Surveys in Geophysics*, *32*(4–5), 585–602. https://doi.org/10.1007/s10712-011-9119-1

Cleveland, R. B., Cleveland, W. S., McRae, J. E., and Terpenning, I. (1990). STL: A seasonal-trend decomposition procedure based on loess. *Journal of Official Statistics*, 6(1), 3–73.

Collilieux, X., and Wöppelmann, G. (2011). Global sea-level rise and its relation to the terrestrial reference frame. *Journal of Geodesy*, *85*(1), 9–22. https://doi.org/10.1007/s00190-010-0412-4

Douglas, B. C. (2001). Sea level change in the era of the recording tide gauge. In B. C. Douglas, M. S. Kearney, and S. P. Leatherman (Eds.), *Sea Level Rise. International Geophysical Servies,* 75, 37–64, *San Diego, California: Academic Press*. https://doi.org/https://doi.org/10.1016/S0074-6142(01)80006-1

Firing, Y. L., Merrifield, M. A., Schroeder, T. A., and Qiu, B. (2004). Interdecadal sea level fluctuations at Hawaii. *Journal of Physical Oceanography*, *34*(11), 2514–2524. https://doi.org/10.1175/JPO2636.1

Fletcher, C., Boyd, R., Neal, W. J., and Tice, V. (2010). Living on the shores of Hawai'i: Natural Hazards, the environment, and our communities. *Honolulu, Hawaii: University of Hawai'i Press*, 1–371.

Francis, O. P., Panteleev, G. G., and Atkinson, D. E. (2011). Ocean wave conditions in the Chukchi Sea from satellite and in situ observations. *Geophysical Research Letters*, *38,* L24610. https://doi.org/10.1029/2011GL049839

Gazeaux, J., Williams, S., King, M., Bos, M., Dach, R., Deo, M., et al. (2013). Detecting offsets in GPS time series: First results from the detection of offsets in GPS experiment. *Journal of Geophysical Research: Solid Earth*, *118*(5), 2397–2407. https://doi.org/10.1002/jgrb.50152

Good, S. A., Martin, M. J., and Rayner, N. A. (2013). EN4: Quality controlled ocean temperature and salinity profiles and monthly objective analyses with uncertainty estimates. *Journal of Geophysical Research: Oceans*, *118*(12), 6704–6716. https://doi.org/10.1002/2013JC009067

Hackl, M., Malservisi, R., Hugentobler, U., and Wonnacott, R. (2011). Estimation of velocity uncertainties from GPS time series: Examples from the analysis of the South African TrigNet network. *Journal of Geophysical Research: Solid Earth*, *116,* B11404. https://doi.org/10.1029/2010JB008142

Hassani, H. (2007). Singular spectrum analysis: methodology and momparison. *Journal of Data Science*, *5*, 239–257.

Holgate, S. J., Matthews, A., Woodworth, P. L., Rickards, L. J., Tamisiea, M. E., Bradshaw, E., et al. (2013). New data systems and products at the permanent service for mean sea level. *Journal of Coastal Research*, 29(3), 493–504. https://doi.org/10.2112/JCOASTRES-D-12-00175.1

Kalnay, E., Kanamitsu, M., Kistler, R., Collins, W., Deaven, D., Gandin, L., et al. (1996). The NCEP/NCAR 40-year reanalysis project. *Bulletin of the American Meteorological Society*, *77*(3), 437–472. https://doi.org/10.1175/1520-0477(1996)077<0437:TNYRP>2.0.CO;2

Leuliette, E. W., and Miller, L. (2009). Closing the sea level rise budget with altimetry, Argo, and Grace. *Geophysical Research Letters*, *36,* L04608. https://doi.org/10.1029/2008GL036010

Mao, A., Harrison, C. G. A., and Dixon, T. H. (1999). Noise in GPS coordinate time series.

Journal of Geophysical Research: Solid Earth, *104*(B2), 2797–2816. https://doi.org/10.1029/1998JB900033

McDougall, T. J., and Barker, P. M. (2011). *Getting started with TEOS-10 and the Gibbs Seawater (GSW) Oceanographic Toolbox*, 28pp, SCOR/IAPSO WG127, ISBN 978-0-646-55621-5.

Mertz, F., Pujol, M.-I., and Faugère, Y. (2018). Product user manual (Version 4.0). Copernicus Marine Environment Monitoring Service. Retrieved from http://cmems-resources.cls.fr/documents/PUM/CMEMS-SL-PUM-008-032-051.pdf

Moore, J. G. (1970). Relationship between subsidence and volcanic load, Hawaii. *Bulletin Volcanologique*, *34*(2), 562–576. https://doi.org/10.1007/BF02596771

Moore, J. G. (1987). Subsidence of the Hawaiian ridge. In R. W. Decker, T. L. Wright, and P. H. Stauffer (Eds.), *Volcanism in Hawaii, U.S. Geological Survey Professional Pape*r, 1350, 85-100, *Reston, Virginia*

Peltier, W. R., Argus, D. F., and Drummond, R. (2015). Space geodesy constrains ice age terminal deglaciation: The global ICE-6G_C (VM5a) model. *Journal of Geophysical Research: Solid Earth*, *120*, 450–487. https://doi.org/10.1002/2014JB011176

Permanent Service for Mean Sea Level (PSMSL). (2018). Tide Gauge Data. Retrieved from https://www.psmsl.org/data/obtaining/

Pujol, M.-I., and Sea Level Thematic Center Team. (2017). Quality information document. Copernicus Marine Environment Monitoring Service. Retrieved from http://apdrc.soest.hawaii.edu/doc/CMEMS-SL-QUID-008-032-051.pdf

Rebischung, P., and Schmid, R. (2016). IGS14/igs14.atx: a new framework for the IGS products, American Geophysical Union Fall Meeting, San Francisco, CA.

Romine, B. M., Fletcher, C. H., Barbee, M. M., Anderson, T. R., and Frazer, L. N. (2013). Are beach erosion rates and sea-level rise related in Hawaii? *Global and Planetary Change*, *108*, 149–157. https://doi.org/10.1016/j.gloplacha.2013.06.009

Santamaría-Gómez, A., Gravelle, M., Dangendorf, S., Marcos, M., Spada, G., and Wöppelmann, G. (2017). Uncertainty of the 20th century sea-level rise due to vertical land motion errors. *Earth and Planetary Science Letters*, *473*, 24–32. https://doi.org/https://doi.org/10.1016/j.epsl.2017.05.038

Santamaría-Gómez, A., Gravelle, M., and Wöppelmann, G. (2014). Long-term vertical land motion from double-differenced tide gauge and satellite altimetry data. *Journal of Geodesy*, *88*(3), 207–222. https://doi.org/10.1007/s00190-013-0677-5

Save, H., Bettadpur, S., and Tapley, B. D. (2016). High-resolution CSR GRACE RL05 mascons. *Journal of Geophysical Research: Solid Earth*, *121*(10), 7547–7569. https://doi.org/10.1002/2016JB013007

Swenson, S., Chambers, D., and Wahr, J. (2008). Estimating geocenter variations from a combination of GRACE and ocean model output. *Journal of Geophysical Research: Solid Earth*, *113,* B08410. https://doi.org/10.1029/2007JB005338

Wang, G., and Soler, T. (2015). Measuring land subsidence using GPS : ellipsoid height versus orthometric height. *Journal of Surveying Engineering*, *141*(2), 05014004. https://doi.org/10.1061/(ASCE)SU.1943-5428.0000137

Wang, X., Cheng, Y., Wu, S., and Zhang, K. (2016). An enhanced singular spectrum analysis method for constructing nonsecular model of GPS site movement. *Journal of Geophysical Research: Solid Earth*, *121*(3), 2193–2211. https://doi.org/10.1002/2015JB012573

Woodworth, P. L., and Player, R. (2003). The permanent service for mean sea level: an update to

the 21st century. *Journal of Coastal Research*, *19*(2), 287–295. Retrieved from http://www.jstor.org/stable/4299170

Wöppelmann, G., and Marcos, M. (2016). Vertical land motion as a key to understanding sea level change and variability. *Reviews of Geophysics*, *54*(1), 64–92. https://doi.org/10.1002/2015RG000502

Yang, L., Wang, G., Bao, Y., Kearns, T. J., and Yu, J. (2016a). Comparisons of ground-based and building-based CORS: a case study in the region of Puerto Rico and the Virgin Islands. *Journal of Surveying Engineering*, *142*(3), 05015006. https://doi.org/10.1061/(ASCE)SU.1943-5428.0000155

Yang, L., Wang, G., Huérfano, V., von Hillebrandt-Andrade, C. G., Martínez-Cruzado, J. A., and Liu, H. (2016b). GPS geodetic infrastructure for natural hazards study in the Puerto Rico and Virgin Islands region. *Natural Hazards*, *83*(1), 641–665. https://doi.org/10.1007/s11069-016-2344-7

Zhang, J., Bock, Y., Johnson, H., Fang, P., Williams, S., Genrich, J., et al. (1997). Southern California permanent GPS geodetic array: Error analysis of daily position estimates and site velocities. *Journal of Geophysical Research: Solid Earth*, *102*(B8), 18035–18055. https://doi.org/10.1029/97JB01380

List of Figures